metals

MDPI

Article

Advancements in Hybrid Additive Manufacturing: Integrating SLM and LMD for High-Performance Applications

Deviprasad Chalicheemalapalli Jayasankar *, Stefan Gnaase, Maximilian Alexander Kaiser, Dennis Lehnert and Thomas Tröster

Mechanical Department, University of Paderborn, Warburger Strasse 100, 33098 Paderborn, Germany; stefan.gnaase@uni-paderborn.de (S.G.); maximilian.kaiser@uni-paderborn.de (M.A.K.); dennis.lehnert@uni-paderborn.de (D.L.); thomas.troester@uni-paderborn.de (T.T.)
* Correspondence: deviprasad.jayasankar@uni-paderborn.de; Tel.: +49-5251-60-5938

Abstract: Additive manufacturing (AM) technologies enable near-net-shape designs and demand-oriented material usage, which significantly minimizes waste. This points to a substantial opportunity for further optimization in material savings and process design. The current study delves into the advancement of sustainable manufacturing practices in the automotive industry, emphasizing the crucial role of lightweight construction concepts and AM technologies in enhancing resource efficiency and reducing greenhouse gas emissions. By exploring the integration of novel AM techniques such as selective laser melting (SLM) and laser metal deposition (LMD), the study aims to overcome existing limitations like slow build-up rates and limited component resolution. The study's core objective revolves around the development and validation of a continuous process chain that synergizes different AM routes. In the current study, the continuous process chain for DMG MORI Lasertec 65 3D's LMD system and the DMG MORI Lasertec 30 3D's was demonstrated using 316L and 1.2709 steel materials. This integrated approach is designed to significantly curtail process times and minimize component costs, thus suggesting an industry-oriented process chain for future manufacturing paradigms. Additionally, the research investigates the production and material behavior of components under varying manufacturing processes, material combinations, and boundary layer materials. The culmination of this study is the validation of the proposed process route through a technology demonstrator, assessing its scalability and setting a benchmark for resource-efficient manufacturing in the automotive sector.

Keywords: additive manufacturing (AM); selective laser melting (SLM); laser metal deposition (LMD); hybrid manufacturing; process optimization; 316L; 1.2709

check for updates

Citation: Chalicheemalapalli Jayasankar, D.; Gnaase, S.; Kaiser, M.A.; Lehnert, D.; Tröster, T. Advancements in Hybrid Additive Manufacturing: Integrating SLM and LMD for High-Performance Applications. *Metals* **2024**, *14*, 772. https://doi.org/10.3390/met14070772

Academic Editor: Guido Di Bella

Received: 20 May 2024
Revised: 25 June 2024
Accepted: 26 June 2024
Published: 29 June 2024

Copyright: © 2024 by the authors. Licensee MDPI, Basel, Switzerland. This article is an open access article distributed under the terms and conditions of the Creative Commons Attribution (CC BY) license (https://creativecommons.org/licenses/by/4.0/).

1. Introduction

Additive manufacturing, also known as 3D printing, is a transformative technology that is shaping the future of production across various industries. This process involves creating objects layer-by-layer using computer-aided design (CAD) models, which allows for the construction of both simple and complex structures [1,2]. Over the years, researchers have expanded the scope of additive manufacturing by developing new techniques and materials suitable for a range of applications. One of the most significant benefits of additive manufacturing is its ability to produce customized products at relatively low costs. Unlike traditional manufacturing processes that often require costly molds and have high material wastage, 3D printing minimizes waste by using only the necessary amount of material to build parts [1]. This not only makes it more environmentally friendly but also cost-effective, especially for small-scale production.

Fields such as the aerospace and automotive industries, medicine, electronics and civil engineering have greatly benefited from the advancements in additive manufacturing [3]. For instance, in the aerospace industry, the ability to produce lightweight components can

lead to significant fuel savings [4]. In the medical field, custom prosthetics and implants can be tailored to individual patients, improving outcomes and comfort [5–7]. Moreover, the continuous improvement in 3D printing technologies has made these machines more accessible and affordable, fostering innovation and allowing for rapid prototyping and manufacturing. This evolution from rapid prototyping to rapid manufacturing signifies a shift towards using 3D printing for full-scale production, which can dramatically alter manufacturing processes and lead to more efficient, cost-effective and customized production capabilities [8–10]. In the current study, the focus on both selective laser melting (SLM) and laser metal deposition (LDM) processes is particularly relevant due to their renowned accuracy and precise material deposition capabilities [11]. These characteristics make them highly suitable for applications where precision is critical, such as in the aerospace, automotive, and medical industries. SLM is advantageous for its ability to create parts with complex geometries and excellent mechanical properties from metallic powders. SLM achieves this by fully melting the metal powder, layer by layer, using a high-powered laser beam. This process allows us to produce parts with a density close to 100%, making them particularly strong and durable. In the SLM process, several types of lasers are utilized, each offering unique advantages for specific applications. Fiber lasers, which use an optical fiber doped with rare-earth elements like ytterbium, are favored for their high power, excellent beam quality, and efficiency, making them ideal for detailed and complex parts [12]. Diode lasers, although less common in SLM due to lower beam quality, are compact, efficient, and cost-effective for specific material applications [13]. Ytterbium lasers, a subset of fiber lasers, provide high-intensity beams suitable for efficiently melting metallic powders. Nd lasers, which utilize a neodymium-doped crystal, offer high peak power and precision, beneficial for specialized manufacturing processes, though they are less frequently used for metal SLM.

LDM, on the other hand, is highly regarded for its ability to repair or add material to existing components, as well as fabricate new parts directly from metal powders or wire [14]. LDM uses a laser to melt the feed material as it is being deposited onto a substrate, creating high-quality metal layers. This method is particularly valued for its application in part repair and refurbishment, which can significantly extend the service life of high-value components. Like SLM, LMD also employs various types of lasers, each chosen for its specific advantages in material processing. Fiber lasers, using an optical fiber doped with rare-earth elements like ytterbium, are highly favored for their excellent beam quality, high power, and efficiency, making them ideal for precise and detailed material deposition [15]. Despite the significant advantages of both SLM and LDM, each technology carries inherent limitations that can influence their suitability for various manufacturing applications [16–19]. SLM, known for its precision, suffers from a slower build rate because it involves fully melting fine metal powders [20,21]. This requires careful control over several parameters such as laser power, speed, and the build chamber environment, ensuring the structural integrity and resolution of the part but at the cost of production speed. LDM allows for a faster deposition rate as larger quantities of material can be melted and deposited in a shorter time. However, it generally achieves lower resolution and less dimensional accuracy than SLM [22–24]. LDM's primary challenge is its inability to reach the fine detail that SLM can achieve, due to the larger size of the deposited material and the spread of the melt pool.

In response to these challenges, the current study proposes a process chain that strategically combines both SLM and LDM to leverage the strengths of each method while compensating for their weaknesses. This hybrid approach employs SLM to produce sections of a component requiring high resolution and dimensional accuracy, such as intricate internal channels or complex geometries. LDM, in contrast, is used in areas of the component where high resolution is less critical, but where speed of production is essential. This includes the bulk sections of a part or areas where structural integrity and material properties are more crucial than fine detail. By implementing LDM in these regions, the overall build time of the component can be significantly reduced without

sacrificing the quality and functionality of the critical areas manufactured using SLM. This integrated approach not only optimizes the manufacturing process by reducing time and material waste but also enhances the functionality of the final product by tailoring different sections of the component to specific performance requirements or different materials. This methodological synergy is particularly beneficial in industries such as aerospace and automotive, where the complexity and performance demand of components often necessitate both high precision and efficient production rates.

2. Materials and Methods

2.1. Material Selection

To achieve an integrated manufacturing solution utilizing both SLM and LDM processes, it is critical to select a material that not only exhibits compatibility with both techniques but also holds significant industrial relevance. In the current study, the selection has been directed towards metals due to their extensive application across diverse sectors. Among the metals often employed in additive manufacturing, stainless steel (specifically grades 316L and 304), titanium alloy (Ti-6Al-4V), aluminum alloy (AlSi10Mg), nickel-based alloys (Inconel 625 and 718), cobalt chrome, and tool steels (such as 1.2709) are predominant. These materials are preferred for their unique properties that cater to specific industrial needs. Both 316L stainless steel and 1.2709 tool steel have demonstrated excellent processability in SLM and LDM. They maintain structural integrity and achieve high density and fine feature resolutions in SLM, while LDM's capability to deposit these steels ensures effective repairs and enhancements without compromising the material's innate properties.

While materials like titanium and nickel-based alloys bring specific benefits, their higher cost can be prohibitive. In contrast, 316L and 1.2709 offer a cost-effective alternative without compromising on essential attributes such as strength, durability, and corrosion resistance. This makes them financially viable for a broad array of applications. 316L stainless steel is particularly valued in sectors that demand stringent hygienic conditions and high corrosion resistance, such as the food, medical, and marine industries. On the other hand, 1.2709 tool steel is favored in environments that require high strength and resistance to thermal fatigue, making it ideal for aerospace and high-performance tooling applications. By centering on 316L stainless steel and 1.2709 tool steel, this study capitalizes on the materials' extensive industrial acceptance and their versatility in adapting to both SLM and LDM technologies. This focused approach ensures that the manufacturing solution not only meets diverse industry standards but also remains economically and technologically sustainable.

2.2. Sample Production

To validate the proposed methodology, small scale samples were fabricated. Crucial to this process chain was ensuring accurate positioning of the samples across various systems to maintain stringent manufacturing tolerances. To ensure a smooth transition between SLM and LMD, a surface milling stage was integrated using a conventional machining tool. This stage serves a dual purpose: it helps mitigate the buildup of inaccuracies from previous processes, and it creates a flat contact surface that is crucial for achieving strong adhesion at the interface between subsequent manufacturing stages. To facilitate this transition seamlessly, the movement of samples between the LMD system (DMG MORI LT65 3D) and the conventional machine (DMG MORI Ultrasonic 65 MB) is efficiently managed by digitally transferring the workpiece zero point through a zero-point clamping system. This setup ensures that each phase in the manufacturing process aligns perfectly, enhancing the overall integrity and quality of the final product. This transition required a designed connection to the machine table. Given that the conventional machining components are not suited for the high temperatures (up to 400 °C) prevalent in additive manufacturing, a cooling platform was essential to shield them. The design for the zero-point clamping system and the cooling platform was developed using the CAD software SolidWorks 2020 by Dassault Systèmes, as depicted in Figure 1.

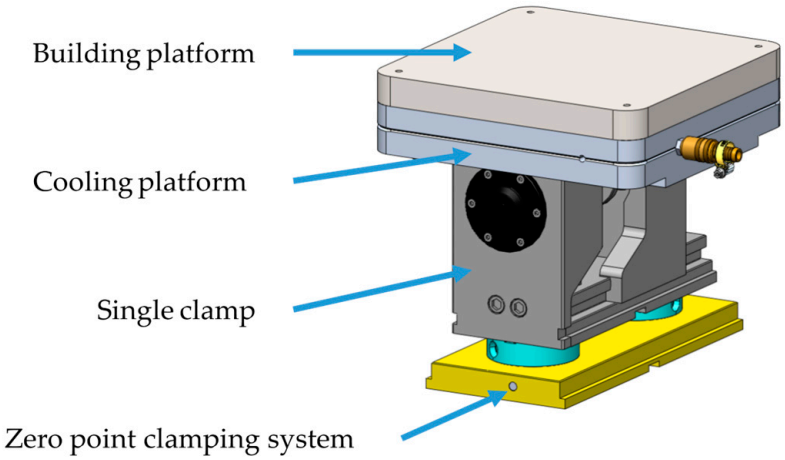


Figure 1. CAD model of clamping module with cooling and building platform.

Furthermore, maintaining tight tolerance integration between the LMD system and the conventional 5-axis machining center necessitated precise alignment of the build platform in the SLM system. Challenges arose due to the SLM system's build platform lacking a mechanically defined positioning system, compounded by the integrated camera's significant barrel distortion which precluded accurate position determination. To overcome these obstacles, digital image correlation (DIC) techniques were employed, utilizing the Aramis 5M system from GOM GmbH. This involved using reference points measured in relation to each other according to spatial directions with dedicated software. A manual correlation between the build platform, the machine frame, and the machine's coordinate system was then performed to ensure consistent and production-oriented positioning of the build platform across the entire process chain. The measurement procedure for the SLM system's building platform is detailed in Figure 2. This defined approach ensures the integration of the DMG Mori SLM system within the proposed production process chain, enhancing overall production accuracy and efficiency.

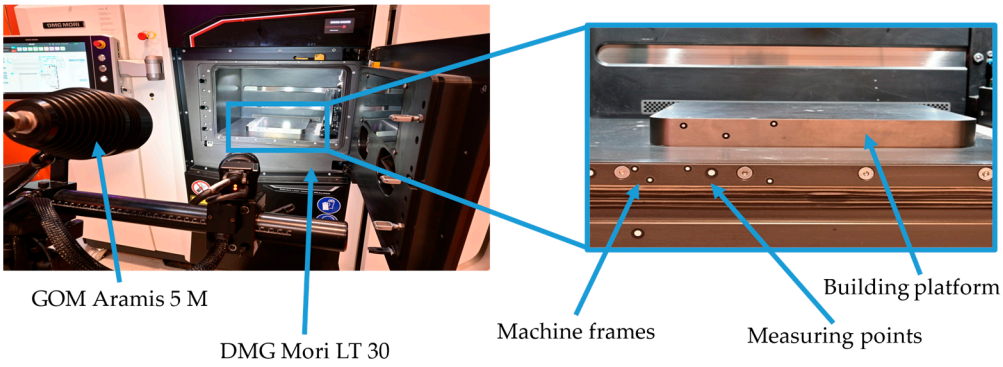


Figure 2. Image showing the DIC setup used to align the build platform.

After integrating the machines into a controlled coordinate process chain, the samples were produced in four distinct configurations as depicted in Table 1. Specifically, in the table "Material-1" and "Material-2" refer to the primary materials used in the study, which are 1.2709 tool steel and 316L stainless steel, respectively. Table 2 presents the supplier-provided mechanical properties of the materials. "Interface material" denotes the material used at the interface between Material-1 and Material-2 to enhance the bonding and mechanical properties. The use of an interface material is critical for ensuring a robust transition between different materials, thus optimizing the overall performance of the hybrid components. Table 3 presents the process parameters used for producing the samples according to their respective manufacturing techniques.

Table 1. Sample types produced using the proposed process.

Type/Strategy	Material-1/Process	Interface Material	Material-2/Process	Remarks
1	1.2709/SLM	-	1.2709/LDM	Same materials
2	1.2709/SLM	-	316L/LDM	Different materials
3	1.2709/SLM	1.2709/LDM	316L/LDM	Same material at interface
4	1.2709/SLM	316L/LDM	1.2709/LDM	Different material at the interface

Table 2. Mechanical properties of the material used in the study.

Tensile Strength/MPa	Yield Strength/MPa	Elongation at Break/%	Hardness/HV10	Surface Roughness/Ra
		1.2709		
1095	945	11	550	5
		316L		
605	550	45	215	6

Table 3. Production parameters used to produce the samples.

SLM	LMD
■ Layer thickness: 50 µm ■ Laser power: 275 W ■ Exposure speed: 0.75 m/s ■ Hatch distance: 0.115 mm	■ Strategy: spiral from the inside to the outside alternating + contour with 0 mm offset ■ Laser power: 1800 W followed by 100 W per shift reduced until 1200 W were reached ■ Traversing speed: 1000 mm/min ■ Traversing speed: 1000 mm/min ■ Powder mass flow rate: 12 g/min ■ Minimum shift time: 100 s ■ Layer thickness: 0.9 mm
■ Laser: YLR-1000-WC	■ Laser: LMD3000-60 × 3 kW
■ DMG MORI LT30 SLM 2nd Gen Single Laser; Bielefeld, Germany; year of construction: 2018	■ DMG MORI LT65 3D, Pfronten; Germany; year of construction: 2017

Cylindrical samples with a diameter of 10 mm and a height of 100 mm were produced. In the initial fabrication approach (Strategies 1 and 2), a component was constructed with a first section of 50 mm using SLM. The subsequent 50 mm of the component was completed using LMD, without incorporating an intermediate material layer. For the alternate fabrication approach (Strategies 3 and 4), the process began similarly with a 50 mm section constructed using SLM. However, this was followed by the addition of a 9 mm intermediate layer using LMD. The remaining portion of the component, another 50 mm, was completed using LMD, resulting in a total height that is 9 mm greater than that of Strategies 1 and 2. Following the production phase, a comprehensive series of tests were conducted to assess the machinability, mechanical, and metallographic properties of the samples. These tests are critical for evaluating the efficacy of the chosen AM routes, ensuring that the final products meet the required specifications and performance standards.

3. Results and Discussion

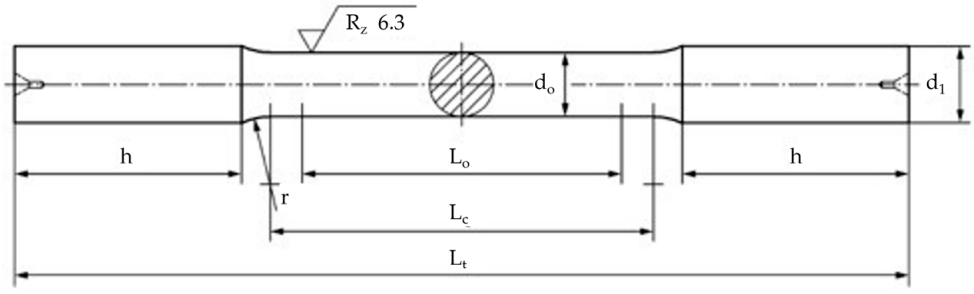
To validate the reliability of the proposed process, a detailed examination of the samples is conducted, beginning with the characterization of mechanical properties. This initial step is critical for establishing a baseline understanding of the sample's performance under stress. Following this, hardness tests are performed, providing further insight into the material's structural integrity and resistance to deformation. In addition to these

physical properties, the microstructural characteristics of the materials and process routes are meticulously analyzed. This analysis is conducted using both a light microscope and a scanning electron microscope (SEM). Electron backscatter diffraction (EBSD) is employed as the primary technique in SEM analyses to provide detailed information on the crystallographic orientation and grain structure, which are crucial for understanding the material's mechanical behavior and potential failure modes.

Due to the multi-material composition of the samples, which includes different steel alloys, careful post-processing is essential to ensure that the subsequent tests are performed without introducing defects associated with the post-processing stage. This involves identifying and applying optimal machining parameters that are specifically tailored to the characteristics of the selected materials and their respective manufacturing techniques. Ensuring that these parameters are finely tuned guarantees that the overall quality of the multi-material components is preserved. This is vital not only for the reliability of the test results but also for the components' practical applicability in real-world scenarios, where material performance under operational stresses and environmental conditions is critical.

3.1. Post-Processing

The combination of two manufacturing processes with different material combinations represents a changed boundary condition for this, which requires adjustments to the machining parameters of the post-processing. During the post-processing (milling), a roughing process was first carried out using an indexable insert with a 35° chisel. The feed rate was 0.15 mm/rev with a cutting speed of 39 m/min and an infeed of the chisel of 0.3 mm. The different stiffnesses of the materials resulted in a clear vibration behavior of the specimens (chatter). The chatter marks on the sample surface showed that the classic machining parameters had to be adjusted. After extensive adjustment tests, the desired form and dimensional accuracy could be achieved by means of an additional finishing process with lower feed rates of 0.08 mm/rev and a cutting speed of 25 m/min and an infeed of only 0.08 mm. With these adjustments, the samples were successfully prepared for subsequent testing, meeting the required specifications with a standard deviation of ±0.03 mm in diameter, suitable for comprehensive evaluation in accordance with DIN 50125 as shown in Figure 3 [25]. For Strategies 1 and 2, after machining, the sections fabricated using SLM and LMD each measure 46 mm. In contrast, for Strategies 3 and 4, the machined component consists of 41.5 mm sections for both SLM and LMD, along with a 9 mm intermediate layer.



- d_o – Gauge diameter
- d_1 – Head diameter ($d_1 \geq 1.2\ d_o$)
- h – Head Length
- r– Radius ($r \geq 0.75\ d_o$)
- L_o – Initial Measuring length ($L_o \geq 5d_o$)
- L_c – Parallel Length ($L_c \geq L_c + d_o$)
- L_t – Total Length

d_o	L_o	d_1	r	h	L_c	L_t
6	30	8	5	25	36	92

Figure 3. Tensile test sample dimensions with cylindrical cross-section used in the current study.

3.2. Mechanical Characterization

The mechanical properties of the multi-material specimens were thoroughly evaluated through tensile tests, conducted on cylindrical specimens with a diameter of 6 mm and a parallel length of 36 mm. These tests adhered to the standards outlined in DIN EN ISO 6892-1 [26], with specimen preparation compliant with DIN 50125 [25]. Testing was performed on a Zwick Z250 machine, equipped with hydraulically clamped jaws exerting a clamping pressure of 30 bar. The quasi-static tensile tests proceeded at a speed of 2 mm/min, equivalent to an average strain rate of 0.001 1/s. To capture and analyze the deformation behavior of the specimens, digital image correlation (DIC) was utilized. This technique allowed for the precise tracking of local deformations, providing insightful data on how the material combinations and process variations influenced mechanical properties. The strains mapped onto the specimens, displayed in the principal stress direction, illuminated the deformation behaviors and regions of necking as shown in Figure 4. The gray areas in Figure 4 indicate the locations near the samples clamped area during testing. Due to the clamping, data from these regions were not recorded, which is why these areas are not represented in the color legend. Notably, in all experimental setups, the material of lower strength, specifically 316L stainless steel, exhibited the greatest strains, with specimen failures predominantly occurring in these regions.

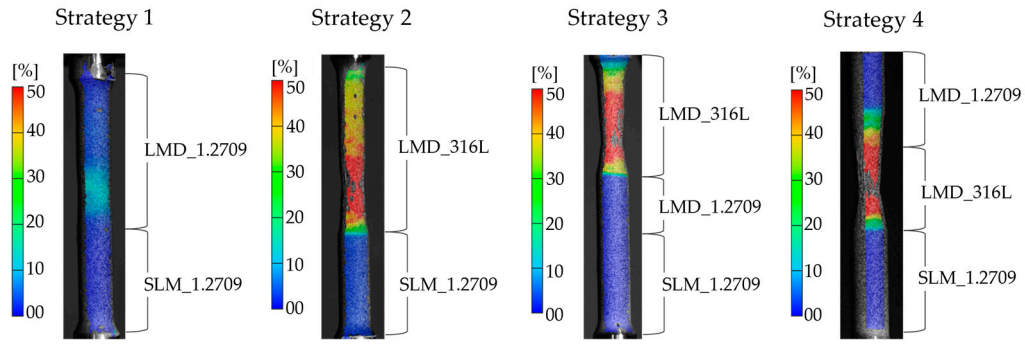
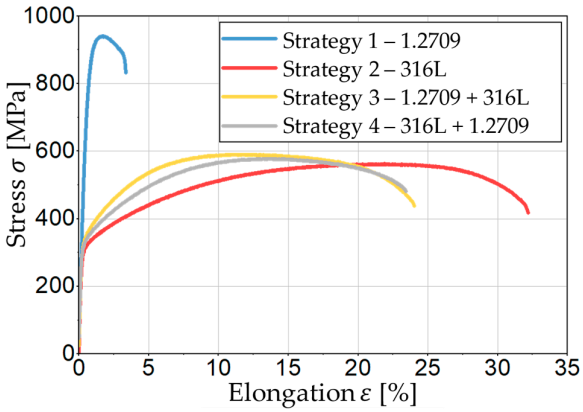


Figure 4. DIC image showing the principal stresses with respect to strain rate.

In particular, in the mono-material specimens from strategy 1, failure consistently occurred in the center, within the section fabricated using the LMD process. This highlighted a distinct difference in the mechanical properties achieved by SLM versus LMD for the same material, 1.2709 tool steel. Crucially, the results demonstrated that the interfaces between the different materials and processes did not experience critical strains nor contribute to failure, suggesting robust mechanical integration of the materials.

Additionally, stress–strain diagrams were generated from the collected data to visually represent the material behaviors under stress, as depicted in Figure 5, which shows a single iteration of results. Each test was repeated three times to validate data reliability. Derived mechanical characteristic values, including standard deviations based on three samples each, are further illustrated in Figure 6. These diagrams confirmed that the mechanical properties of the hybrid constructs were predominantly dictated by the weaker material, 316L stainless steel. Specimens incorporating a higher proportion of 316L (strategies 2–4) not only showed reduced overall strength but also exhibited significantly higher elongation. For instance, strategy 2, which had the highest proportion of 316L, displayed the most substantial elongation at over 30%, coupled with the lowest strength at 560 MPa. Conversely, a higher ratio of 1.2709 (strategy 1) resulted in higher strength and reduced elongation, with the mono-material sample combining SLM and LMD processes showing strength up to 950 MPa and elongation below 5%, highlighting a limited plastic range between yield and ultimate tensile strength.



Test method
Quasi-static tensile test
Test standard
DIN 50125
Test speed
2 mm/min
Specimen geometry
Round tensile specimen
Deformation measurement
GOM Aramis M5
Specimen production
Combined AM method
Test temperature
20 °C (room temperature)

Figure 5. Stress–strain curves derived from tensile testing of cylindrical samples produced using different strategies.

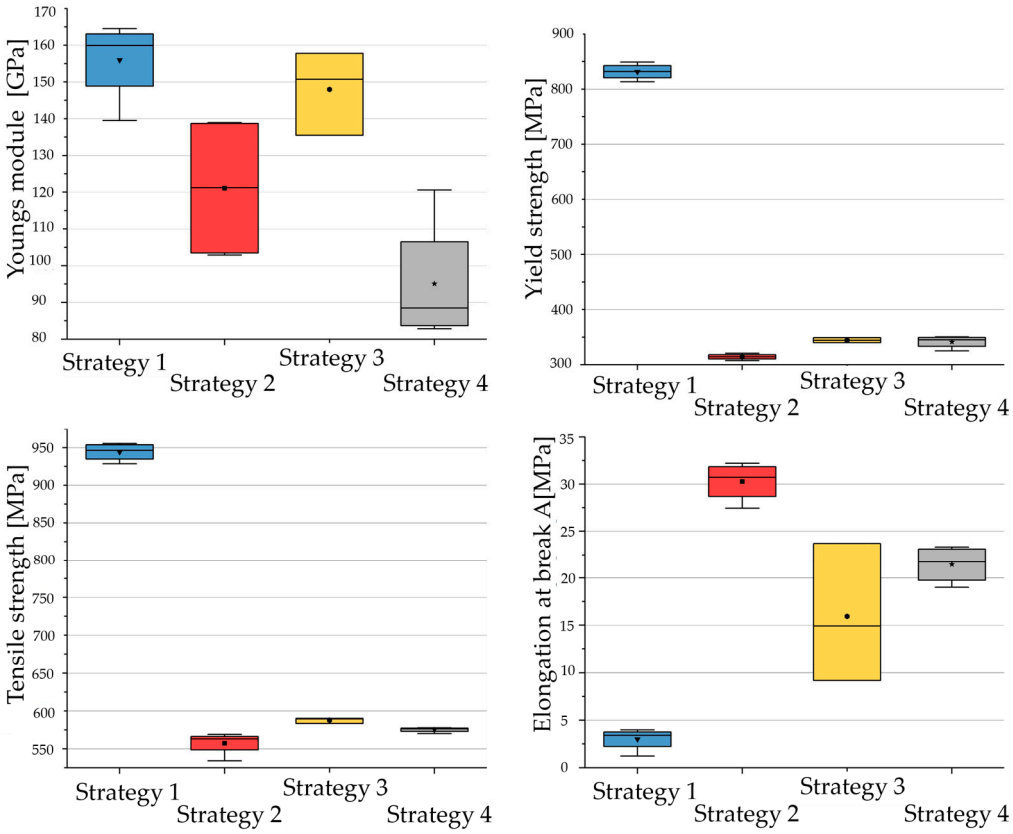


Figure 6. Mechanical properties of samples with respect to different strategies.

3.3. Hardness Measurement

To assess the relative, local strengths of the samples, a Vickers hardness test was conducted in accordance with DIN EN ISO 6507-1 [27]. The testing was performed using an ATM Carat 930 fully automatic hardness testing machine. This macro hardness test was executed under a standard load of 49.03 N (HV5), with the test force applied for a duration of 10 s at each measurement point. The indent used was a diamond pyramid with a tip angle of 136°. Given the length of the additive manufactured samples, measuring them in a single clamping was not feasible. Consequently, each sample was sectioned into five parts using a sample separator, ensuring that the interfaces were contained within a single segment. The samples were then cold-embedded and polished as per material specifications. One of the results from these tests are detailed in Figure 7, where between 78 and 101 impressions were made per sample, spaced 0.9 mm apart. The hardness results

presented reflect a single iteration of the tests. To ensure accuracy and reliability, hardness tests were conducted on three different samples for each strategy. For each designated point (location/area) on the sample, five readings were recorded along the vertical axis (perpendicular to the length), resulting in a total of 15 data points per location across the three samples.

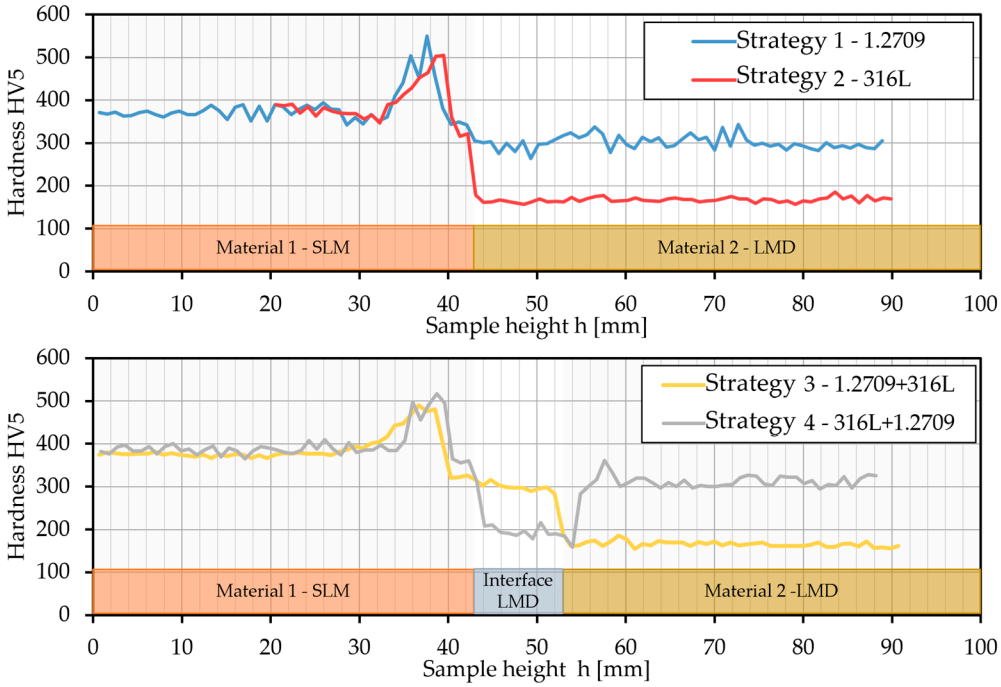


Figure 7. Hardness properties of samples with respect to different strategies.

In the results, Material 1, which is 1.2709 steel produced via SLM, showed an average hardness of 377 HV5, with a standard deviation of 11 HV5. The additional layering by LMD on the SLM structure led to an increase in hardness of the 1.2709 by up to 180 HV5 from a height of 32 mm. The process-induced heat treatment from the LMD's high temperatures caused a noticeable inhomogeneity in hardness along the component, akin to what is observed in welding processes. Moreover, Figure 7 illustrates that hardness is influenced by both the material and the manufacturing process. For instance, the average hardness of the 1.2709 base material fabricated using SLM was 377 HV5, while the same material processed through LMD averaged 300 HV5, indicating a 20.42% reduction in hardness. The 316L stainless steel, solely produced using LMD, also showed variability in hardness based on the manufacturing strategy. When used as an intermediate layer in strategy 4 (316L + 1.2709), the hardness was 30 HV5 higher compared to its use in strategies 2 and 4 (both 316L and 316L + 1.2709). This difference likely results from the slightly higher heat capacity of the 1.2709, which extends the thermal impact on the 316L during processing.

3.4. Microstructure

As a next step, the microstructure of the samples was analyzed. Images of the microstructure were captured using a Keyence VHX-5000 from KEYENCE DEUTSCHLAND GmbH (Neu-Isenburg, Germany) and are presented in Figure 8. To enhance the visibility of the microstructure, the samples underwent a four-minute etching in etchant before being cleaned with ethanol. A comparative analysis of the microstructures of 1.2709 steel processed by SLM and LMD reveals significant grain refinement in the SLM components, which correlates with their higher mechanical strength compared to the LMD-fabricated structures of the same material. This grain refinement results in an increased number of dislocations within the component, contributing to greater resistance to plastic deformation and thereby enhancing tensile strength. The influence of heat introduced by the LMD

process on the SLM components is also distinctly visible, with the heat-affected zone clearly marked by etching and noticeable grain coarsening upon closer examination.

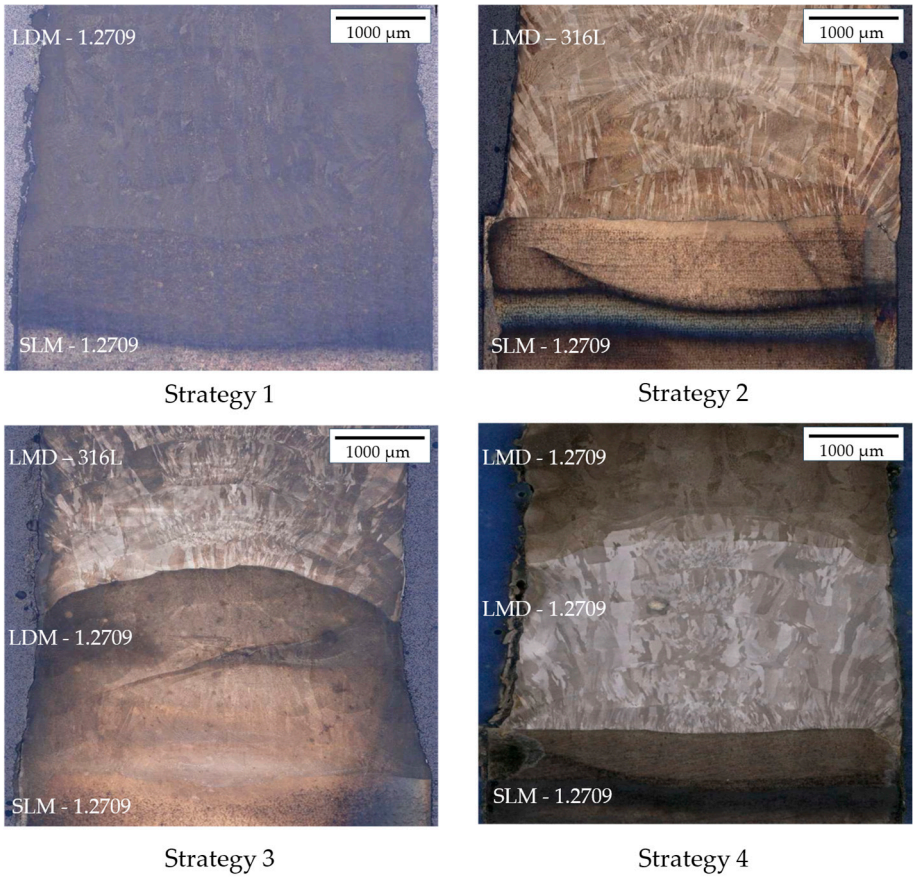


Figure 8. Microstructure images of samples with respect to different strategies.

Further structural insights, particularly regarding crystal structure and orientation at the boundary layers, were obtained through electron backscatter diffraction (EBSD) measurements conducted using a Zeiss Gemini from Carl Zeiss Microscopy Deutschland GmbH. The analysis (shown in Figure 9) reveals a pronounced preferred direction of grain growth in the build direction for both SLM and LMD processes. Notably, in LMD, grains grow to a length of at least 200 µm, significantly larger than the SLM grains, which measure only 70 µm—a 300% increase in size. This disparity emphasizes the mechanical and structural differences observed under the light microscope. Figure 9a also indicates that the 1.2709 in the SLM-fabricated areas adopts a partially martensitic structure, with fine martensite needles visible, likely due to the heat treatment from the energy used in the LMD process. Furthermore, during the EBSD analysis (shown in Figure 9b), it was noted that the SLM structure of 1.2709 exhibits a body-centered cubic (BCC) crystal lattice, while the LMD structure of 316L displays a face-centered cubic (FCC) crystal lattice. The resolution limitations of EBSD at the grain boundaries occasionally led to incorrect assignment of these boundaries to another crystal structure. Ultimately, EBSD allows for a much more precise examination of the boundary layer between different areas than is possible with an optical microscope. Despite the machined surfaces, interactions between the different material layers of 1.2709 and 316L were detected in the SEM. The re-melting of the SLM-produced 1.2709 due to the energy input from the LMD laser beam results in a bond at the boundary layer, demonstrating a microscopic form of closure which elucidates the strength of the bond at this interface.

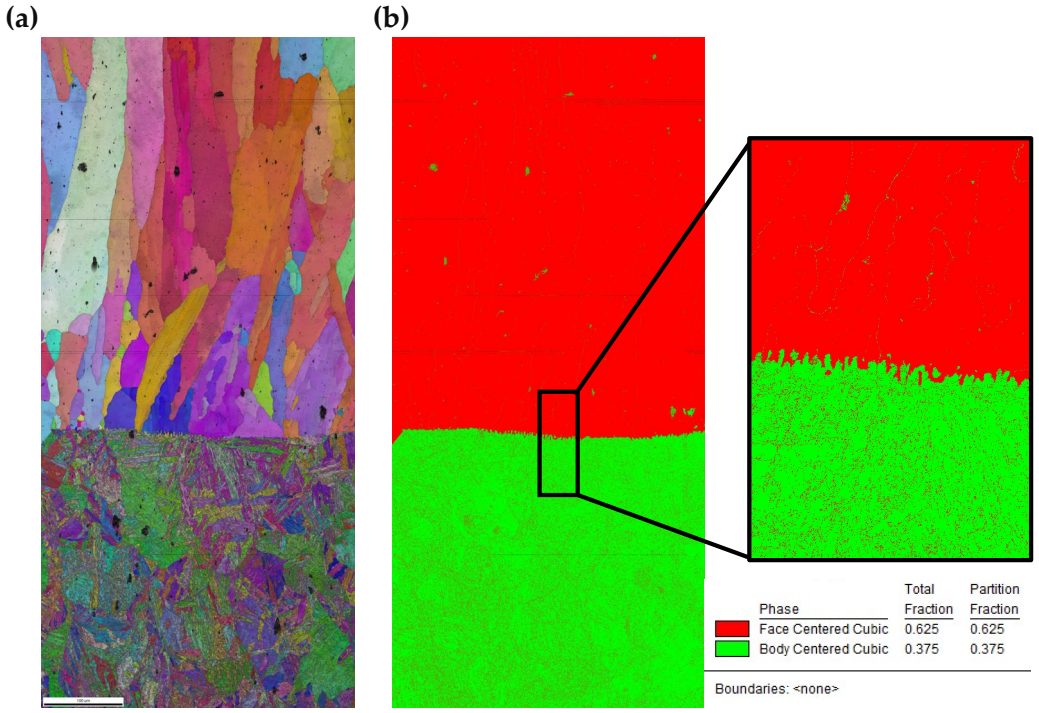


Figure 9. EBSD measurement of the boundary layer of strategy 2 (SLM_1.2709 + LMD 316L) showing (**a**) crystal orientation and (**b**) crystal structure.

4. Conclusions

In conclusion, the current study demonstrates the successful integration of selective laser melting (SLM) and laser metal deposition (LMD) in a multi-AM route to fabricate complex, application-specific components. The use of materials such as 316L stainless steel and 1.2709 tool steel, compatible with both SLM and LMD, has proven effective in achieving the necessary mechanical properties and structural integrity for high-performance applications. The study highlights the precision of SLM in creating intricate, highly stressed areas, while LMD excels in rapidly constructing larger, less detail-oriented sections, enhancing both the efficiency and cost-effectiveness of production. Additionally, the application of advanced manufacturing techniques like DIC and EBSD has provided deep insights into material properties and boundary interactions, reinforcing the strength at the interfaces between different materials.

The successful creation of a technology demonstrator further validates the practical utility of the multi-AM approach, underscoring the transformative potential of additive manufacturing in industrial design. This demonstration showcases significant advancements in tool longevity and performance, particularly for tools used in non-isothermal hot forming processes, a critical area in automotive manufacturing. Overall, the research promotes the broader adoption and development of hybrid additive manufacturing techniques, suggesting a promising future to produce complex, high-performance components that require flexibility, efficiency, and precision.

Author Contributions: Conceptualization, S.G. and M.A.K. Data curation, S.G. and M.A.K. Formal analysis, M.A.K. Funding acquisition, T.T. Investigation, S.G. and M.A.K. Methodology, S.G. and M.A.K. Project administration, D.L. and T.T. Resources, M.A.K. Software, S.G. Supervision, D.L. and T.T. Validation, M.A.K. Writing—original draft, D.C.J. Writing—review and editing, D.C.J. and D.L. All authors have read and agreed to the published version of the manuscript.

Funding: This research was funded by the State of North Rhine–Westphalia (Programm für rationelle Energieverwendung, regenerative Energien und Energiesparen) under Progress.nrw—research program/progres.nrw: 005-2112-0061_0226.

Data Availability Statement: The data presented in this study are available on request from the corresponding author due to privacy/legal concerns.

Acknowledgments: The authors would like to extend their gratitude to the laboratory technicians of the LiA Chair for their invaluable assistance. We would also like to express our gratitude to the LWK Chair for their invaluable support and contributions to this work.

Conflicts of Interest: The authors declare no conflicts of interest. The funders had no role in the design of the study; in the collection, analyses, or interpretation of data; in the writing of the manuscript; or in the decision to publish the results.

References

1. Bhatia, A.; Sehgal, A.K. Additive manufacturing materials, methods and applications: A review. *Mater. Today Proc.* **2021**, *81*, 1060–1067. [CrossRef]
2. TNgo, D.; Kashani, A.; Imbalzano, G.; Nguyen, K.T.; Hui, D. Additive manufacturing (3D printing): A review of materials, methods, applications and challenges. *Compos. Part B Eng.* **2018**, *143*, 172–196.
3. Rouf, S.; Malik, A.; Singh, N.; Raina, A.; Naveed, N.; Siddiqui, M.I.H.; Haq, M.I.U. Additive manufacturing technologies: Industrial and medical applications. *Sustain. Oper. Comput.* **2022**, *3*, 258–274. [CrossRef]
4. Najmon, J.C.; Raeisi, S.; Tovar, A. Review of additive manufacturing technologies and applications in the aerospace industry. *Addit. Manuf. Aerosp. Ind.* **2019**, 7–31. [CrossRef]
5. Salmi, M. Additive Manufacturing Processes in Medical Applications. *Materials* **2021**, *14*, 191. [CrossRef] [PubMed]
6. Ghomi, E.R.; Khosravi, F.; Neisiany, R.E.; Singh, S.; Ramakrishna, S. Future of additive manufacturing in healthcare. *Curr. Opin. Biomed. Eng.* **2021**, *17*, 100255.
7. Javaid, M.; Haleem, A. Additive manufacturing applications in medical cases: A literature based review. *Alex. J. Med.* **2019**, *54*, 411–422. [CrossRef]
8. Thomas, D. Costs, benefits, and adoption of additive manufacturing: A supply chain perspective. *Int. J. Adv. Manuf. Technol.* **2015**, *85*, 1857–1876. [CrossRef] [PubMed]
9. Atzeni, E.; Iuliano, L.; Marchiandi, G.; Minetola, P.; Salmi, A.; Bassoli, E.; Denti, L.; Gatto, A. *Additive Manufacturing as a Cost-Effective Way to Produce Metal Parts*; CRC Press: Boca Raton, FL, USA, 2014.
10. Busachi, A.; Erkoyuncu, J.; Colegrove, P.; Martina, F.; Watts, C.; Drake, R. A review of Additive Manufacturing technology and Cost Estimation techniques for the defence sector. *CIRP J. Manuf. Sci. Technol.* **2017**, *19*, 117–128. [CrossRef]
11. BGraf; Schuch, M.; Kersting, R.; Gumenyuk, A.; Rethmeier, M. Additive Process Chain using Selective Laser Melting and Laser Metal Deposition. In Proceedings of the Lasers in Manufacturing Conference 2015, Munich, Germany, 22–25 June 2015.
12. Colopi, M.; Demir, A.G.; Caprio, L.; Previtali, B. Limits and solutions in processing pure Cu via selective laser melting using a high-power single-mode fiber laser. *Int. J. Adv. Manuf. Technol.* **2019**, *104*, 2473–2486. [CrossRef]
13. Hori, E.; Sato, Y.; Shibata, T.; Tojo, K.; Tsukamoto, M. Development of SLM process using 200 W blue diode laser for pure copper additive manufacturing of high density structure. *J. Laser Appl.* **2021**, *33*, 012008. [CrossRef]
14. Mahamood, R. *Laser Metal Deposition Process of Metals, Alloys, and Composite Materials*; Springer: Berlin/Heidelberg, Germany, 2018.
15. Froend, M.; Ventzke, V.; Riekehr, S.; Kashaev, N.; Klusemann, B.; Enz, J. Microstructure and microhardness of wire-based laser metal deposited AA5087 using an Ytterbium fibre laser. *Mater. Charact.* **2018**, *143*, 59–67. [CrossRef]
16. Methani, M.M.; Cesar, P.F.; de Paula Miranda, R.B.; Morimoto, S.; Özcan, M.; Revilla-León, M. Additive Manufacturing in Dentistry: Current Technologies, Clinical Applications, and Limitations. *Curr. Oral Health Rep.* **2020**, *7*, 327–334. [CrossRef]
17. Ahuja, B.; Karg, M.; Schmidt, M. Additive manufacturing in production: Challenges and opportunities. In Proceedings of the Laser 3D Manufacturing II, San Francisco, CA, USA, 7–12 February 2015.
18. Lemu, H.G. On Opportunities and Limitations of Additive Manufacturing Technology for Industry 4.0 Era. In *Advanced Manufacturing and Automation VIII*; Springer: Singapore, 2018.
19. Taborda, L.L.L.; Maury, H.; Pach, J. Design for additive manufacturing: A comprehensive review of the tendencies and limitations of methodologies. *Rapid Prototyp. J.* **2021**, *27*, 918–966. [CrossRef]
20. Sefene, E.M. State-of-the-art of selective laser melting process: A comprehensive review. *J. Manuf. Syst.* **2022**, *63*, 250–274. [CrossRef]
21. Yap, C.Y.; Chua, C.K.; Dong, Z.L.; Liu, Z.H.; Zhang, D.Q.; Loh, L.E.; Sing, S.L. Review of selective laser melting: Materials and applications. *Appl. Phys. Rev.* **2015**, *2*, 041101. [CrossRef]
22. Ghosal, P.; Majumder, M.C.; Chattopadhyay, A. Study on direct laser metal deposition. *Mater. Today Proc.* **2018**, *5*, 12509–12518. [CrossRef]
23. Ansari, M.; Jabari, E.; Toyserkani, E. Opportunities and challenges in additive manufacturing of functionally graded metallic materials via powder-fed laser directed energy deposition: A review. *J. Mater. Process. Technol.* **2021**, *294*, 117117. [CrossRef]
24. Tseng, S.-F.; Hung, T.-Y.; Chang, C.-M. Mechanical and microstructural properties of additively manufactured Ti–6Al–4 V stents with CO2 laser post annealing treatment. *Int. J. Adv. Manuf. Technol.* **2022**, *119*, 6571–6581. [CrossRef]

25. *DIN 50125:2016-12*; Testing of Metallic Materials—Tensile Specimens. Deutsches Institut Fur Normung E.V.: Berlin, Germany, 2016.
26. *DIN EN ISO 6892-1*; Metallic Materials—Tensile Testing—Part 1: Method of Test at Room Temperature. Deutsches Institut Fur Normung E.V.: Berlin, Germany, 2019.
27. *ISO 6507-1:2022*; Metallic Materials—Vickers Hardness Test—Part 1: Test Methods. Deutsches Institut Fur Normung E.V.: Berlin, Germany, 2022.

Disclaimer/Publisher's Note: The statements, opinions and data contained in all publications are solely those of the individual author(s) and contributor(s) and not of MDPI and/or the editor(s). MDPI and/or the editor(s) disclaim responsibility for any injury to people or property resulting from any ideas, methods, instructions or products referred to in the content.